

# Production of Light Element Primary Process nuclei in neutrino-driven winds

A. Arcones

*Institut für Kernphysik, TU Darmstadt, Schlossgartenstr. 9, 64289 Darmstadt, Germany*

*GSI Helmholtzzentrum für Schwerionenforschung, Planckstr. 1, 64291 Darmstadt, Germany*

*Department of Physics, University of Basel, Klingelbergstraße 82, 4056, Basel, Switzerland*

F. Montes

*Joint Institute for Nuclear Astrophysics, <http://www.jinaweb.org>*

*National Superconducting Cyclotron Laboratory, Michigan State University, East Lansing, MI 48824, USA*

## ABSTRACT

We present first comparisons between Light Element Primary Process (LEPP) abundances observed in some ultra metal poor (UMP) stars and nucleosynthesis calculations based on long-time hydrodynamical simulations of core-collapse supernovae and their neutrino-driven wind. UMP star observations indicate  $Z \geq 38$  elements include the contributions of at least two nucleosynthesis components: r-process nuclei that are synthesized by rapid neutron capture in a yet unknown site and LEPP elements (mainly Sr, Y, Zr). We show that neutrino-driven wind simulations can explain the observed LEPP pattern. We explore in detail the sensitivity of the calculated abundances to the electron fraction, which is a key nucleosynthesis parameter but poorly known due to uncertainties in neutrino interactions and transport. Our results show that the observed LEPP pattern can be reproduced in proton- and neutron-rich winds.

*Subject headings:* nuclear reactions, nucleosynthesis, abundances — Galaxy: abundances — supernovae: general

## 1. Introduction

Elements heavier than iron are mainly produced by the slow (s-) and rapid (r-) neutron capture processes. In contrast to the s-process, for which the astrophysical environments are identified (Busso et al. 1999; Straniero et al. 2006), the r-process site(s) remains unknown (Arnould et al. 2007). There are some indications that more than one component or site contributes to the abundances of the so called r-process elements (Wasserburg et al. 1996; Qian & Wasserburg 2001; Truran et al. 2002; Travaglio et al. 2004; Aoki et al. 2005; Otsuki et al. 2006; Montes et al. 2007). Most of the recent progress in understanding the origin of elements commonly associated with the r-process is due to observations of ultra metal-poor (UMP) stars (see Sneden et al. 2008, for a recent review). The elemental abundances observed in the atmosphere of these very old stars come from a few events. These stars generally present a robust pattern for “heavy” elements  $56 < Z < 83$ , in agreement with the expected contribution of the r-process to the solar system, but show some scatter for “light” elements  $Z < 47$  (Johnson & Bolte 2002; Sneden et al. 2008). This suggests that at least two types of primary nucleosynthesis events contribute to the abundances of those elements.

The first indication for these two nucleosynthesis components came from meteoritic data on  $^{129}\text{I}$  and  $^{182}\text{Hf}$  (Wasserburg et al. 1996). The idea of the different components was later extended to account for all abundances in metal-poor stars in the phenomenological model of Qian & Wasserburg (2001, 2007). They argued that supernovae from low-mass progenitors with  $8M_{\odot} < M < 12M_{\odot}$  (H-source in their terminology) lead to all “heavy” and some “light” elements, and that explosions of more massive progenitors,  $12M_{\odot} < M < 25M_{\odot}$  (L-source), contribute to the remaining light  $A < 130$  elements. A similar conclusion was reached independently by Montes et al. (2007) using a slightly different pattern for the L-source (LEPP source in their terminology).

The abundances of star HD 122563 (Westin et al. 2000) were used to build an L-source pattern. This star shows mainly elements produced in the L-source with small contamination from the H-source, characterized by the abundances observed in CS 22892-052 (Sneden et al. 2003). While Qian & Wasserburg (2007) assumed that all material above  $Z = 56$  in HD 122563 was produced by the H-source, Montes et al. (2007) used a smaller H-source contribution responsible for all the abundance of elements heavier than  $Z = 62$ . Montes et al. (2007) discussed the assumption that HD 122563 is representative of the L-source by showing a hint of robustness of the observed pattern of UMP stars. However, more observations of L-source enriched (or r-process poor) UMP stars are needed before a definitive conclusion is reached. In this paper, the LEPP (or L-source) pattern was taken from Qian & Wasserburg (2008) based on the abundances of Honda et al. (2006). It covers elements in the range

$38 < Z < 47$  and it is assumed to be robust.

More recently, Qian & Wasserburg (2008) updated their two-component model to include a third component producing Fe but not  $Z \geq 38$  elements. The need for an additional component resulted from using newer higher-resolution data that included many stars with  $[\text{Fe}/\text{H}] \leq -3$  where the amount of Fe (produced originally only in the L-source) relative to Sr (produced in both L- and H- sources) was too large compared to the yields based on the two-component model.

The process leading to elements with  $A < 130$  (L-source) has been called in the literature the weak r-process (Truran & Cowan 2000), charged-particle reaction (CPR) process (Woosley & Hoffman 1992; Freiburghaus et al. 1999; Qian & Wasserburg 2007), and Lighter Element Primary Process (LEPP) (Travaglio et al. 2004; Montes et al. 2007). In this paper, we refer to this process as LEPP because it does not make any reference to the specific nuclear reactions or astrophysical environment. The term LEPP was first introduced in Travaglio et al. (2004) which used a galactic chemical evolution model to search for the astrophysical environments producing the elements Sr, Y, and Zr. Using their s-process model and standard r-process contributions, they found that non-negligible abundances of several isotopes ( $^{86}\text{Sr}$ ,  $^{93}\text{Nb}$ ,  $^{96}\text{Mo}$ ,  $^{100}\text{Ru}$ ,  $^{104}\text{Pd}$ ,  $^{110}\text{Cd}$ ) were still unexplained. Montes et al. (2007) showed that the LEPP elemental abundances that result from using the Travaglio et al. (2004) model are in agreement, within the observational error bars, with the modified abundances of HD 122563 (Fig. 5 in Montes et al. (2007)). The contribution of the LEPP to the solar abundances depends on the s-process model. If further refinements to s-process models eliminate or change the need for a LEPP contribution to the solar system abundances, the apparent agreement between the “solar” LEPP and the UMP observations would have been coincidental. In that case the LEPP may only contribute to the abundances of a few metal-poor stars.

After the initial success of Woosley et al. (1994) in reproducing observed r-process abundances<sup>1</sup>, core-collapse supernovae and the subsequent neutrino-driven winds became one of the most promising candidates for the production of r-process elements because their extreme explosive conditions are very close to the ones needed for the r-process (see e.g., Hoffman et al. 1997; Thompson et al. 2001; Otsuki et al. 2000). Moreover, galactic chemical evolution models favor core-collapse supernovae, since they occur early and frequently enough to account for the abundances observed in old halo stars and in the solar system (Ishimaru & Wanajo 1999; Ishimaru et al. 2004). Although the necessary conditions to pro-

---

<sup>1</sup>Recent work of Roberts et al. (2010) suggests that the high wind entropies obtained at that time could have been due to problems with the equation of state.

duce heavy elements ( $A > 130$ ) are identified (Meyer et al. 1992) (high entropies, low electron fractions, and short expansion timescales), these are not found in the most recent long-time supernova simulations (Pruet et al. 2006; Arcones et al. 2007; Wanajo et al. 2009; Fischer et al. 2010; Hüdepohl et al. 2010).

In this paper we investigate the possibility of producing the LEPP elements in neutrino-driven winds, as suggested by Qian & Wasserburg (2007, 2008). The nucleosynthesis calculations (Sect. 2.3) are based on the spherically symmetric simulations of core-collapse supernovae of Arcones et al. (2007), where the evolution of the neutrino-driven wind was followed during several seconds (Sect. 2.2). Since the neutrino transport in these simulations is only approximate (Scheck et al. 2006), the electron fraction is expected to have some uncertainty as explained in Sect. 2.1. A systematic study of the impact of the wind electron fraction on the nucleosynthesis is included in Sect. 3.1. We show that the nucleosynthesis based on these simulations do not yield heavy r-process nuclei ( $A > 130$ ) but that LEPP elements can be produced in the current neutrino-driven wind models. The different conditions to produce the observed LEPP pattern are investigated in Sect. 3.2. Finally, we conclude and summarize Sect. 4.

## 2. Nucleosynthesis in neutrino-driven winds

When a supernova explodes, matter surrounding the proto-neutron star is heated by neutrinos and expands very fast reaching sometimes even supersonic velocity (Duncan et al. 1986; Thompson et al. 2001). This is known as the neutrino-driven wind and can become neutron or proton rich. The electron fraction  $Y_e$  is determined by the uncertain neutrino properties (energy and luminosity) in the region where neutrinos decouple from matter. This matter near the neutron star consist mainly of neutrons and protons due to the high temperatures in this region. When a mass element expands, its temperature decreases and neutrons and protons recombine to form  $\alpha$ -particles. The density decreases but as the triple-alpha reaction combined with different  $\alpha$  capture reactions are still occurring, heavy seed nuclei may form (Woosley & Hoffman 1992; Wittl et al. 1994). The evolution once the  $\alpha$ -particles start forming heavier nuclei depends on the electron fraction and it will be discussed in detail in Sect. 3.1.

### 2.1. Wind electron fraction

The evolution of the nascent neutron star and the properties of neutrinos emitted from its surface have a direct impact on the wind parameters that are relevant for nucleosynthesis: entropy ( $S$ ), expansion timescale ( $\tau = r/v|_{T \sim 0.5 \text{ MeV}}$ ), and electron fraction.  $S$  and  $\tau$  depend on neutrino energy, neutrino luminosity, and on the evolution of the proto-neutron star as (Qian & Woosley 1996):

$$S \propto L^{-1/6} \epsilon^{-1/3} R_{\text{ns}}^{-2/3} M_{\text{ns}}, \quad (1)$$

$$\tau \propto L^{-1} \epsilon^{-2} R_{\text{ns}} M_{\text{ns}}, \quad (2)$$

where  $L$ ,  $\epsilon$  are the neutrino luminosity and mean energy, respectively, and the dependence on the neutron star properties enters through its radius ( $R_{\text{ns}}$ ) and mass ( $M_{\text{ns}}$ ). The evolution of these quantities is mainly given by the equation of state (EoS) at nuclear densities, which is specially uncertain at high densities, and by the amount of matter accreted onto the proto-neutron star, which is higher for more massive stellar progenitors. Eqs. (1)-(2) indicate that different progenitors with the same neutron star evolution lead to similar wind properties. When neutrino luminosities and energies decrease, the entropy slightly increases favoring the production of heavier elements, but at the same time the expansion timescale increases which counteracts and disfavors their production. Therefore, during the wind phase, relatively small changes in the nucleosynthesis can generally be expected when the absolute values of neutrino properties (i.e.,  $L_{\nu_e} + L_{\bar{\nu}_e}$  and  $\epsilon_{\nu_e} + \epsilon_{\bar{\nu}_e}$ ) are changed. After the initial fast contraction of the proto-neutron star, its radius and mass changes only slightly for  $\gtrsim 1$  s after bounce. The main change to  $S$  and  $\tau$  is then the result of the neutrino luminosity variation as a function of time.

The electron fraction is, contrary to  $S$  and  $\tau$ , determined by the relative variations of electron neutrinos and antineutrinos properties. The exact value of neutrino energies and luminosities depend on the accuracy of the supernova neutrino transport calculations and on details of neutrino interactions at high densities (Rampp & Janka 2000; Mezzacappa et al. 2001). At the high temperatures ( $T \gtrsim 10$  GK) where the nucleosynthesis calculations are started, nuclei are photo-dissociated into neutrons and protons and their abundances are given by  $Y_p = Y_e$  and  $Y_n = 1 - Y_e$ , respectively. The electron fraction is determined by charged-current reactions between neutrinos and nucleons and their inverse reactions:



The evolution of the electron fraction is consequently given by:

$$\frac{dY_e}{dt} = \lambda_{\nu_e n} Y_n - \lambda_{p e} Y_p - \lambda_{\bar{\nu}_e p} Y_p + \lambda_{n e^+} Y_n, \quad (5)$$

where  $\lambda_i$  are the reaction rates for the forward and backward reactions in Eqs. (3)-(4). Neutrino emission reactions are negligible in the wind because their rates rapidly drop with temperature ( $\lambda_{pe/ne+} \propto T^5$ ). Following Qian & Woosley (1996), the equilibrium initial  $Y_e$  in the wind is given by

$$Y_e = \frac{\lambda_{\nu_e,n}}{\lambda_{\nu_e,n} + \lambda_{\bar{\nu}_e,p}} = \left[ 1 + \frac{L_{\bar{\nu}_e} \epsilon_{\bar{\nu}_e} - 2\Delta + 1.2\Delta^2/\epsilon_{\bar{\nu}_e}}{L_{\nu_e} \epsilon_{\nu_e} + 2\Delta + 1.2\Delta^2/\epsilon_{\nu_e}} \right]^{-1}. \quad (6)$$

Here the neutrino absorption rates are used in a simple form (Qian & Woosley 1996) without considering weak magnetism and recoil corrections (Horowitz & Li 1999).  $L_{\nu_e}$  is the neutrino luminosity,  $\epsilon_{\nu_e} = \langle \varepsilon^2 \rangle / \langle \varepsilon \rangle \approx 4.1kT_{\nu_e}$  is the ratio of mean squared neutrino energy ( $\langle \varepsilon^2 \rangle$ ) and mean neutrino energy ( $\langle \varepsilon \rangle$ ), and  $kT_{\nu_e}$  is the neutrino temperature in MeV (and similarly for the antineutrinos),  $\Delta$  denotes the neutron-proton mass difference. This simple expression gives only an estimate of the  $Y_e$  value found by supernova neutrino transport calculations (Fischer et al. 2010). The neutrino two-color plot shown in Fig. 1 illustrates the dependence of the  $Y_e$  on the neutrino energies and luminosities using Eq. (6). It also shows the (anti)neutrino energies obtained 10 s after bounce in wind simulations reported in the literature. The most recent long-time supernova simulations (Hüdepohl et al. 2010; Fischer et al. 2010) obtain lower antineutrino energies compared to the earlier models, leading to proton-rich conditions in the wind.

Neutrino energies depend on the temperature of the medium in the region where neutrinos decouple from matter. This region is known as the neutrinosphere and its location is different for each neutrino flavor and energy. Inside of the neutrinosphere, neutrinos are in the thermal equilibrium by charged-current reactions (Eqs. (3)-(4)). Outside of it, neutrinos escape while their temperature stays almost constant and approximately equal to the temperature at their neutrinosphere. Because neutrons are more abundant than protons in the neutron star, electron neutrinos continue interacting to larger radii and thus to lower temperatures than antineutrinos ( $\varepsilon_{\bar{\nu}_e} \gtrsim \varepsilon_{\nu_e}$ ). The  $\mu$  and  $\tau$  (anti)neutrinos interact only via neutral-current reactions and decouple at smaller radii, therefore their energies are larger. During the first seconds after the explosion, the proto-neutron star deleptonizes and the amount of protons in the outer layers decreases. The electron antineutrino energies are thus expected to get higher than the electron neutrino energies leading to an increase of the ratio  $\varepsilon_{\bar{\nu}_e}/\varepsilon_{\nu_e}$ . New hydrodynamical simulations including detailed neutrino transport (e.g. Hüdepohl et al. 2010) show that this simple picture is not valid as the spectra of electron neutrinos and antineutrinos are rather similar, probably due to neutral-current reactions that act in a similar way on all neutrino flavors and become more important as the neutron star cools (Hüdepohl et al. 2010; Arcones et al. 2008). If electron neutrino and antineutrino energies are similar, the neutron-to-proton mass difference favors a value of  $Y_e > 0.5$  (as shown in Fig. 1) by reducing the antineutrino absorption rate relative to the neutrino rate.

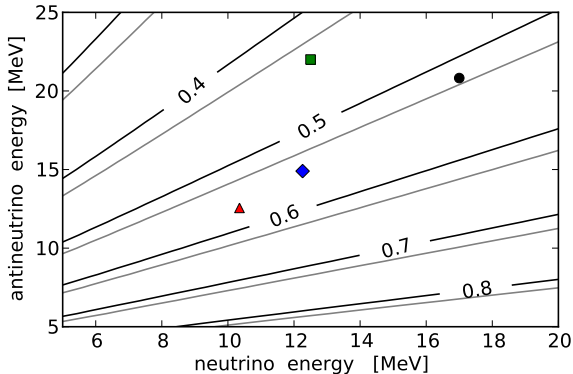


Fig. 1.— Electron fraction based on Eq. (6) for different neutrino (x-axis) and antineutrino (y-axis) energies. The black contours correspond to  $L_{\bar{\nu}_e}/L_{\nu_e} = 1$  and the grey contours to  $L_{\bar{\nu}_e}/L_{\nu_e} = 1.1$ . The symbols show the electron neutrino and antineutrino energies ( $\epsilon_{\nu_e} \approx 4.1kT_{\nu_e}$ ) for different supernova models reported in the literature: square for Woosley et al. (1994), circle for model M15-l1-r6 of Arcones et al. (2007) (note that these models do not include red shift corrections which would reduce the neutrino energies close to the neutron star), triangle for a  $10 M_{\odot}$  progenitor of Fischer et al. (2010), and diamond for Hüpdepohl et al. (2010), all at 10 s after bounce. Adapted from Qian & Woosley (1996).

It should be noted that some uncertainty remain in the calculation of the neutrino spectra. At the high temperatures and densities of the outer layers of the proto-neutron star, there may also be a non-negligible abundance of light nuclei:  $^2\text{H}$ ,  $^3\text{H}$ , and  $^3\text{He}$  (Arcones et al. 2010). These details in the composition are not included in state-of-the-art supernova simulations, although neutrino interactions with these light nuclei have an impact on the neutrino spectra and thus on the  $Y_e$  (Arcones et al. 2008).

## 2.2. Wind simulations

In order to accurately calculate the integrated nucleosynthesis in neutrino-driven winds, the evolution of the supernova ejecta has to be followed for several seconds using hydrodynamical simulations. Such long-term modeling is currently difficult since the supernova explosion mechanism is not yet well understood (Janka et al. 2007; Nordhaus et al. 2010) and it is computationally expensive to perform long-time, multidimensional, systematic studies for different progenitor stars, as would be desirable in nucleosynthesis studies. Ways to overcome these problems include using parametric steady-state wind models (e.g. Thompson et al.

2001) and forcing an explosion by artificially changing neutrinos properties (Messer et al. 2003; Fröhlich et al. 2006a,b; Arcones et al. 2007; Fischer et al. 2010). The evolution of the outflow is rather independent of the details of the explosion mechanism, but depends more on the evolution of the neutron star and on the neutrino emission. Therefore, such approximations are a good basis for nucleosynthesis studies. Although steady-state wind models cannot consistently describe hydrodynamical effects (like the reverse shock and multidimensional instabilities), both approaches agree in the wind phase (Arcones et al. 2007).

For the nucleosynthesis studies in this paper, trajectories, i.e. density and temperature evolutions, from Arcones et al. (2007) were used. These simulations are based on Newtonian hydrodynamics (Scheck et al. 2006; Kifonidis et al. 2006) with general relativistic corrections for the gravitational potential (Marek et al. 2006) combined with a simplified neutrino transport treatment (Scheck et al. 2006), which is computationally very efficient and reproduces the results of Boltzmann transport simulations qualitatively. The neutrino spectra are assumed to follow Fermi-Dirac distributions with spectral temperatures different from the local matter temperature in general. The central part ( $\rho \gtrsim 10^{13} \text{ g/cm}^3$ ) of the proto-neutron star is replaced by a Lagrangian inner boundary placed below the neutrinosphere. This reduces the computational time and is justified in part due to the uncertainties in the high-density EoS. The evolution of the inner boundary is parametrized by its radius and neutrino luminosity. The latter is chosen such that an explosion energy around  $10^{51} \text{ erg}$  is obtained. The neutrino luminosity is constant during the first second after bounce and follows a power law decrease afterwards. We use following models from Arcones et al. (2007): M10-l1-r1 for a  $10M_{\odot}$  progenitor star (hereafter referred as 10M model), M15-l1-r1 (15M model) and M15-l1-r6 (15M(s) model) both for a  $15M_{\odot}$ , and M25-l5-r4 for a  $25M_{\odot}$  (25M model). The proto-neutron star radius and neutrino luminosity evolution are similar for models M10, M15, and M25. Model M15(s) has a significant different proto-neutron star radius contraction but same neutrino luminosity. While the evolution of the inner boundary in model M15 leads to a more compact neutron star (approximately following the behaviour of the EoS from Lattimer & Swesty (1991)), model M15(s) reproduces a neutron star with a larger final radius (similar to the EoS from Shen et al. (1998)). The different compactness of the neutron star implies changes in its radius and mass that directly affect wind parameters (Eqs. (1)–(2)).

The evolution of radius, entropy, temperature, and density is shown in Fig. 2 for a mass element ejected at 5 s after bounce. Since the proto-neutron star in models 10M, 15M, and 25M follows a very similar contraction and neutrino cooling evolution,  $S$  and  $\tau$  of these models and therefore their density and temperature evolution are also similar. Their wind profiles have a small dependence on the mass progenitor. For the most massive progenitor (25M) the proto-neutron star mass becomes larger (due to the higher accretion



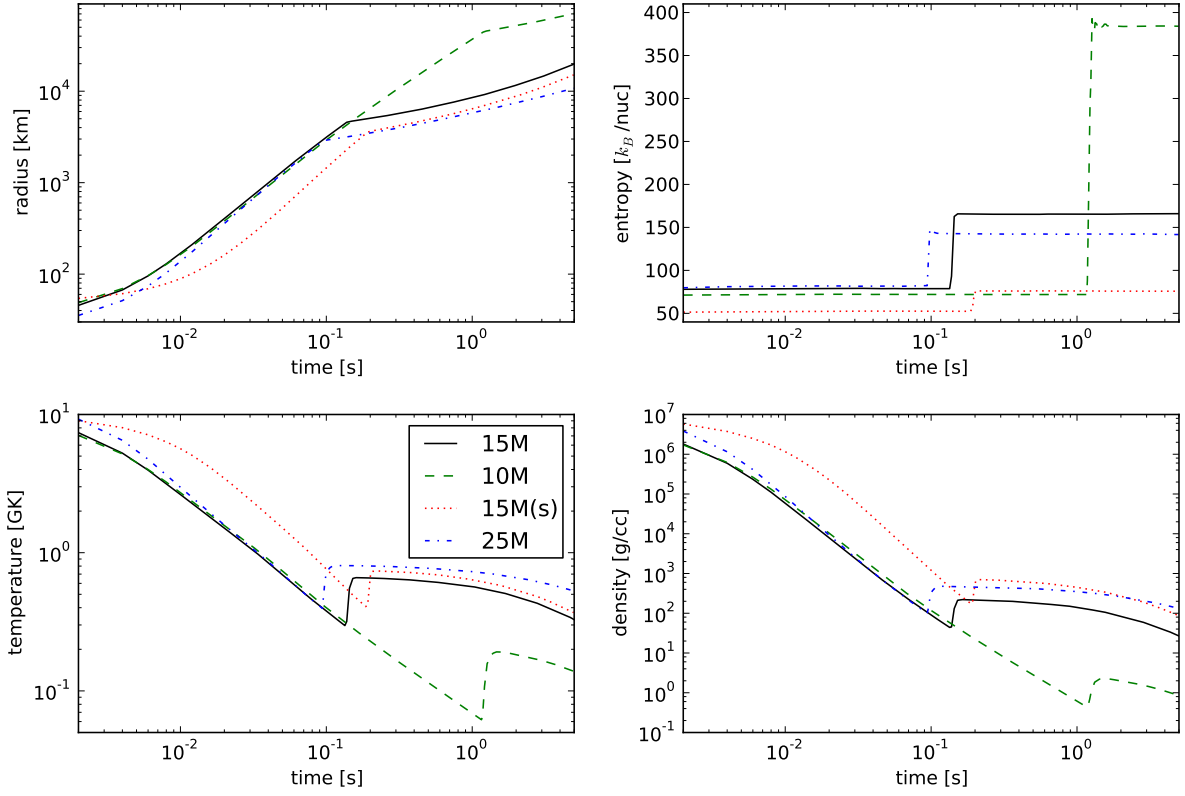


Fig. 2.— Evolution of radius, entropy, temperature, and density of a mass element ejected 5s after bounce for models 10M, 15M, 15M(s), and 25M.

rate) and consequently the wind entropy is also higher than for the less massive progenitors (see Eq. (1)). The impact of varying the progenitor mass becomes however significant in the interaction of the wind with the slowly moving, dense supernova ejecta. This interaction results in a wind termination shock or reverse shock. The behavior of the reverse shock depends on the wind properties, but also on the progenitor structure and anisotropies of the early ejecta (see Arcones et al. (2007); Arcones & Janka (2011) for more details). Model 15M(s), with a slow contracting and less compact proto-neutron star, leads to significantly different wind profiles as shown Fig. 2. The expansion timescale is longer and the wind entropy lower than model 15M (Eqs. 1–2).

### 2.3. Nucleosynthesis network

The evolutions of mass elements ejected between 1 s and 10 s after bounce are used for our nucleosynthesis calculations. The final integrated abundances are calculated by adding the abundances from each mass element weighted by its ejected mass. Each calculation starts when the temperature decreases below 10 GK. The composition is calculated initially by assuming nuclear statistical equilibrium (NSE) for a given initial  $Y_e$ . The evolution of the composition is followed using a full reaction network (Fröhlich et al. 2006b), which includes 4053 nuclei from H to Hf including both neutron- and proton-rich isotopes. Reactions with neutral and charged particles are taken from calculation with the statistical code NON-SMOKER (Rauscher & Thielemann 2000) and experimental rates are included (Angulo et al. 1999, NACRE) when available. The theoretical weak interaction rates are the same as in Fröhlich et al. (2006b). Experimental beta-decay rates are used when available NuDat2 (2009).

## 3. Results

The integrated abundances for the wind models presented in Sect. 2.2 are shown in Fig. 3. The initial electron fraction and neutrino properties ( $L_\nu$  and  $\langle \varepsilon_\nu \rangle$ ) are taken directly from the wind simulations. Based on our simulations, elements are produced up to  $Z = 41$  and no heavy r-process elements can be synthesized. Figure 3 also shows the LEPP elemental pattern from Qian & Wasserburg (2008) normalized to the calculated  $Z = 39$  abundance. As the proto-neutron star evolution and wind properties are very similar in models 10M, 15M, and 25M (see Sect. 2.1), their final abundances are analogous. The impact of the wind parameters ( $S$  and  $\tau$ ) on the abundances can be seen in the right panel of Fig. 3. Models 15M and 15M(s) correspond to the same  $15 M_\odot$  progenitor, but with different proto-neutron star evolution (see Sect. 2.2). For model 15M the wind expansion is faster and the entropy becomes higher than in model 15M(s). Model 15M(s) can produce mainly iron-group nuclei while model 15M leads to heavier nuclei up to  $Z=47$ .

The isotopic production factor indicating the contribution of the ejected isotope to the solar system abundances is defined as,

$$P(i) = \sum_j \frac{M_j}{M_{\text{ej}}^{\text{tot}}} \frac{X_j(i)}{X_\odot(i)}. \quad (7)$$

The sum goes over every mass element and  $M_{\text{ej}}^{\text{tot}}$  is the total ejected mass obtained after subtracting the proto-neutron star mass ( $M_{\text{ns}} \approx 1.4M_\odot$ ) from the progenitor mass.  $X_j(i)$  is the mass fraction of the isotope  $i$  produced in the mass element  $j$ , and  $X_{\odot,i}$  is the mass fraction

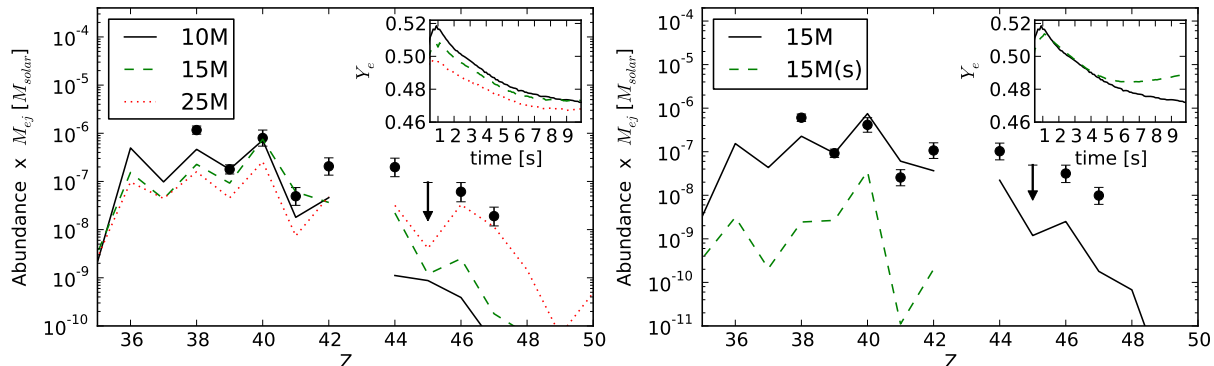


Fig. 3.— Integrated abundances for the models introduced in Sect. 2.2 compared to the LEPP pattern (Qian & Wasserburg 2008) rescaled to  $Z = 39$ . The abundances of different progenitors with a similar evolution of the proto-neutron star are shown in the left panel, while the right panel gives the abundances of the same progenitor with different proto-neutron star evolutions.

of the same isotope  $i$  in the solar system (Lodders 2003). Following Qian & Wasserburg (2008), the solar system was formed from gas with a contribution of core-collapse supernovae of  $M_{\text{gas}} \approx 3.3 \times 10^{10} M_{\odot}$  ejected during  $t \approx 10^{10}$  yr. The rate of all core-collapse supernovae in the Galaxy is  $R_{\text{SN}} \approx 10^{-2} \text{yr}^{-1}$  (Cappellaro et al. 1999). This constrains the amount of a given element  $i$  that can be ejected by a single event. If such an event is representative for all supernovae from different progenitors, this implies that

$$\sum_j \frac{M_j}{M_{\text{ej}}^{\text{tot}}} X_j(i) R_{\text{SN}} t \langle M_{\text{ej}}^{\text{tot}} \rangle \lesssim M_{\text{gas}} X_{\odot}(i), \quad (8)$$

has to be satisfied. Here  $\langle M_{\text{ej}}^{\text{tot}} \rangle$  is the average ejected mass, which can be calculated using Salpeter initial mass function:

$$\langle M_{\text{prog}} \rangle = \frac{\int_8^{25} m^{-2.5} m dm}{\int_8^{25} m^{-2.5} dm} \approx 13 M_{\odot}. \quad (9)$$

Therefore,  $\langle M_{\text{ej}}^{\text{tot}} \rangle = \langle M_{\text{prog}} \rangle - M_{\text{ns}} \simeq 11.5 M_{\odot}$ , assuming that all stars in the range  $8 M_{\odot} < M < 25 M_{\odot}$  contribute. Because the s-process also contributes to the solar system inventory, the production factor has to be smaller than the limit given by Eq. (8):

$$P(i) \lesssim \frac{M_{\text{gas}}}{R_{\text{SN}} t \langle M_{\text{ej}}^{\text{tot}} \rangle} \approx 30. \quad (10)$$

This number is an estimate indicative and comparable with the limit of Mathews et al. (1992) based on the oxygen production in core-collapse supernovae ( $P(i) \lesssim 10$ ).

Production factors are shown in Fig. 4 for all models. The dotted horizontal line indicates the production limit given by Eq. (10). Such limit assumes that every supernova ejects the same amount of matter with the same isotopic composition. If only a subset of supernova (e.g. those from progenitors with masses in a determined range, magnetic fields, etc.) eject those isotopes, the limit will move to larger values. Note that only model 15M(s) does not lead to significant amounts of heavy nuclei because it is producing mainly iron-group nuclei. The overproduction around  $A = 90$  is related with the sudden decrease of the alpha separation energy at magic number  $N = 50$  (see e.g., Woosley et al. 1994; Wittl et al. 1994; Hoffman et al. 1996; Freiburghaus et al. 1999; Hoffman et al. 2008). The production factors reach higher values for low mass progenitors because the relative contribution of mass ejected is higher.

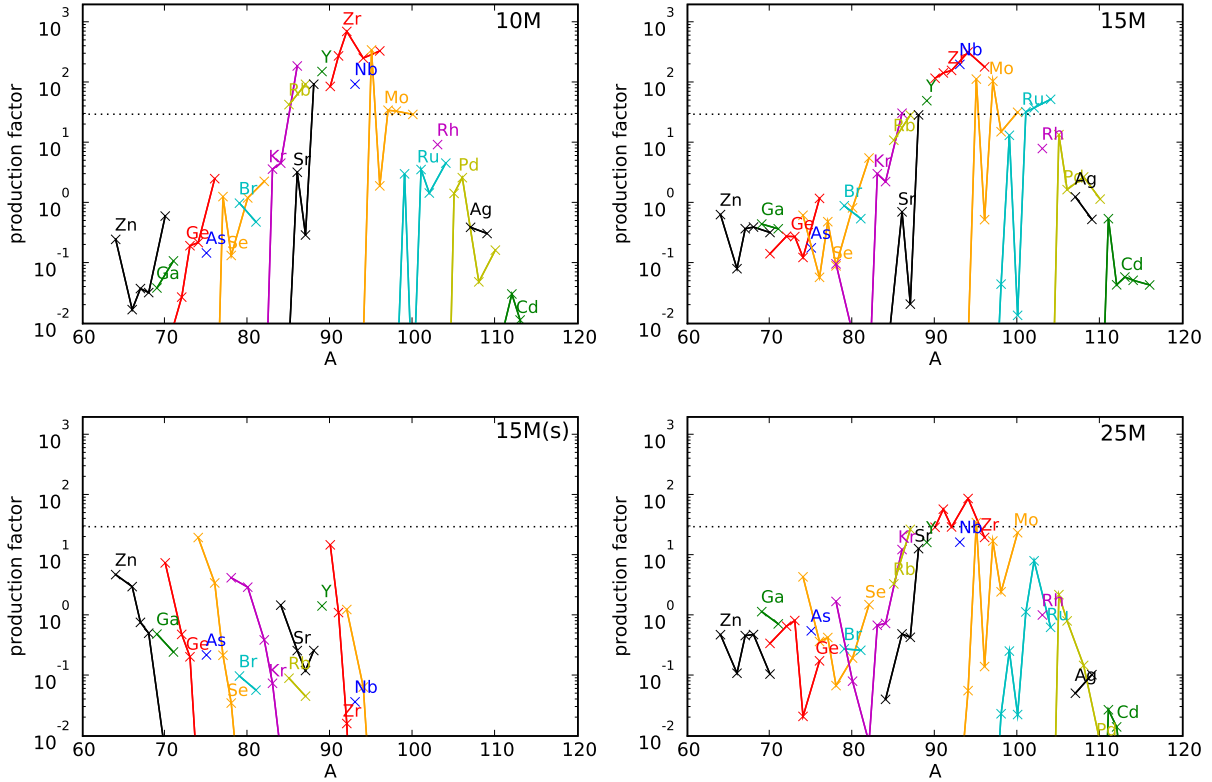


Fig. 4.— Production factor given by Eq. (7) for the different models shown in Fig. 3. The horizontal dotted line marks the overproduction limit. Isotopes for the same element are connected by lines.

### 3.1. Impact of the electron fraction

The electron fraction is extremely sensitive to details of the neutrino interactions and transport, and therefore its exact value is expected to be more uncertain than the value of the other wind parameters. In this section the impact of  $Y_e$  on the production of LEPP elements is explored. In the following, it is assumed that the temperature of the electron antineutrinos is  $kT_{\bar{\nu}_e} \approx 4.5$  MeV. For the electron neutrinos,  $kT_{\nu_e}$  is calculated with Eq. (6) given an initial  $Y_e$ . Neutrino luminosities are kept constant as a function of time for each mass element. For mass element ejected at  $t = 1$  s after bounce,  $L_{\nu_e} = L_{\bar{\nu}_e} \approx 25 \times 10^{51}$  erg s<sup>-1</sup>. Subsequent mass elements have constant luminosities  $L_{\nu}(t) = L_{\nu}(t = 1\text{s})/t^{3/2}$  where  $t$  is the time after core bounce (Arcones et al. 2007). Variations of  $Y_e$  are linked to neutrino properties which also affect  $S$  and  $\tau$ . In the extreme cases where the change in  $Y_e$  is rather large (i.e.,  $Y_e = 0.2$  or  $0.7$ ), the expansion timescale changes only by a factor of two (which does not modify its characteristic timescale of few ms) and the entropy varies by less than 30% (Eqs. (1)-(2)), therefore justifying our approach of keeping  $S$  and  $\tau$  as given by the simulations while varying  $Y_e$ .

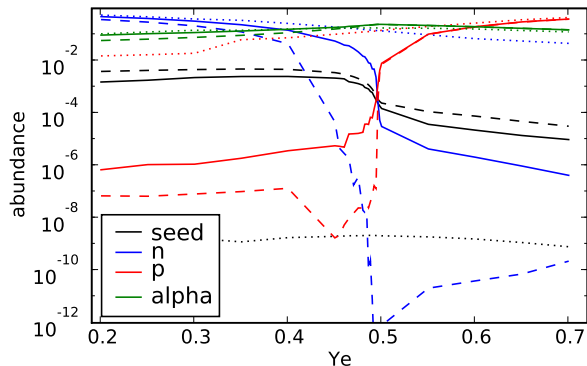


Fig. 5.— Seed nuclei (i.e., nuclei heavier than  $^4\text{He}$ ), neutron, proton, and alpha abundances as a function of  $Y_e$  based on the mass element ejected at 5s after bounce in model 15M. Dotted, solid, and dashed lines correspond to temperatures of 8, 5 and 2 GK, respectively.

The abundances of neutrons, protons,  $\alpha$ -particles, and seed nuclei ( $A > 4$ ) as a function of  $Y_e$  are shown in Fig. 5 for an expanding mass element ejected 5s after bounce of model 15M. The abundance at  $T = 8$  GK consists mainly of nucleons and  $\alpha$ -particles. At  $T = 5$  GK, the abundance of seed nuclei has significantly increased but  $\alpha$ -particles still dominate. Captures of  $\alpha$ -particles drive the creation of heavier nuclei until approximately  $T = 2 - 3$  GK. The composition at this point is very important because the subsequent formation of heavier nuclei depends on the free nucleon-to-seed ratio. Three different  $Y_e$  ranges can be

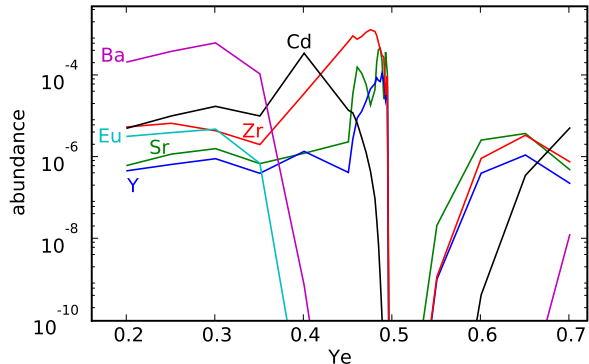


Fig. 6.— Dependence of the abundances of representative elements (Sr, Y, Zr, Cd, Ba and Eu) on the electron fraction. These abundances result from a mass element ejected at 5s after bounce in model 15M.

distinguished in Figs. 5 and 6: proton-rich ( $Y_e > 0.5$ ), rather neutron-rich ( $Y_e \lesssim 0.4$ ), and slightly neutron-rich ( $0.4 \lesssim Y_e \leq 0.5$ ) conditions.

For proton-rich conditions, heavier nuclei are formed by proton and  $\alpha$ -capture reactions for  $T > 3 - 5$  GK. If  $Y_e$  is large, heavier elements can be synthesized for lower temperatures due to the increase of proton and neutron abundances. The amount of neutrons increases with  $Y_e$ , i.e. with the number of free protons (see blue dashed line in Fig. 5). When  $Y_e > 0.5$ , there are always more protons available than what can be captured, and only very few neutrons produced by antineutrino absorption on protons. These neutrons are immediately captured allowing more matter to bypass long-lived isotopes (bottlenecks) such as  $^{64}\text{Ge}$  by  $(n, p)$  reactions in what is known as the  $\nu p$ -process (Fröhlich et al. 2006a,b; Pruet et al. 2006; Wanajo 2006). As the temperature decreases below  $\approx 3$  GK a combination of  $(n, p)$ ,  $(n, \gamma)$ , and  $(p, \gamma)$  reactions carry the flow to heavier nuclei. After charged-particle reactions end, the produced matter decays back to stability, mainly to neutron-deficient isotopes. Only for early mass elements, the reverse shock becomes important since its temperature is still in a relevant range ( $T \approx 2\text{GK}$ ) for the  $\nu p$ -process to occur. The temperature jump at the reverse shock favors thus the production of heavier nuclei. The impact of the reverse shock on the  $\nu p$ -process will be addressed in future work (Wanajo et al. 2010a; Roberts et al. 2010). The heaviest nucleus that can be reached, depends mainly on the specific neutrino luminosities and energies, and in less scale, on entropy and expansion timescale (see Pruet et al. 2006; Wanajo 2006; Martinez-Pinedo et al. 2006), but as shown in Fig. 6, LEPP elements can be produced under proton-rich conditions. As we discussed later, abundances in proton-rich winds are dominated by p-nuclei.

Extreme neutron-rich conditions are naturally more favorable to reach heavy r-nuclei. Although these conditions have not been reproduced in standard supernova ejecta, it may still be possible to obtain them in scenarios such as explosions with high rotation and magnetic fields where a jet forms (Cameron 2001, 2003), or in quark nova (Ouyed et al. 2002; Jaikumar et al. 2007) where a phase transition in the neutron star leads to a direct ejection of very neutron-rich matter. In neutron-rich conditions, the reaction sequence  ${}^4\text{He}(\alpha, \gamma){}^9\text{Be}(\alpha, n){}^{12}\text{C}$  (Woosley & Hoffman 1992; Freiburghaus et al. 1999) followed by  $\alpha$ -captures quickly increases the amount of seed nuclei to amounts larger than in proton-rich conditions as shown in Fig. 5. Once charged-particle freeze-out occurs, nuclei are still driven by neutron-captures and  $\beta$ -decays before the density gets too low and the created matter  $\beta$ -decays towards stability.

When the ejecta are slightly neutron-rich, the  ${}^4\text{He}(\alpha, \gamma)$  sequence starts to compete with the triple alpha-reaction and it dominates for  $Y_e < 0.45$ . Subsequent  $\alpha$ -captures reactions drive the flow following a path close to or at the valley of beta-stability (Woosley & Hoffman 1992; Witti et al. 1994; Freiburghaus et al. 1999). At closed  $N = 50$  neutron shell, the alpha separation energy decreases (Möller et al. 1997) preventing  $\alpha$ -captures to continue with the formation of heavier nuclei. This leads to an accumulation of matter around  ${}^{88}\text{Sr}$ ,  ${}^{89}\text{Y}$ ,  ${}^{90}\text{Zr}$  (Woosley & Hoffman 1992; Witti et al. 1994; Freiburghaus et al. 1999). When the temperature drops below  $\approx 3$  GK, the Coulomb barrier produces the end of  $\alpha$ -reactions and the material captures neutrons if the neutron-to-seed ratio is still high enough. When the matter is symmetric ( $Y_e = 0.5$ ) only elements up to the iron-group are formed.

### 3.2. LEPP and $Y_e$ evolution

For the evolution of the initial electron fraction, we use a parametric approach (similar to Wanajo 2007) with the aim of fitting the abundances observed in LEPP-enriched UMP stars. In the following, model 15M is used unless otherwise specified.

#### 3.2.1. Proton-rich winds

The integrated abundances corresponding to three different  $Y_e$  evolutions are shown in Fig. 7. These evolutions are motivated by the recent results of Hüdepohl et al. (2010) for the explosion and wind evolution of a  $8.8 M_\odot$  stellar progenitor that shows an increasing  $Y_e$  as a function of time. The abundance pattern in the LEPP region  $38 < Z < 47$  changes only slightly for the different cases and fits observations within uncertainties. The robustness of

the abundance pattern can be attributed to the consistency in the  $(p, \gamma)$  and  $(n, p)$  reaction path for the mass elements responsible for the abundances in the LEPP region. Most of those elements are produced when  $Y_e > 0.6$ . Such robustness provides a natural explanation for the consistency of the suggested UMP star abundance LEPP pattern mentioned in Montes et al. (2007). Figure 8 shows the similarity of the abundance pattern for  $Y_e = 0.65$  for two different mass elements ejected at early and late times. The only significant difference is the amount of mass ejected in each case.

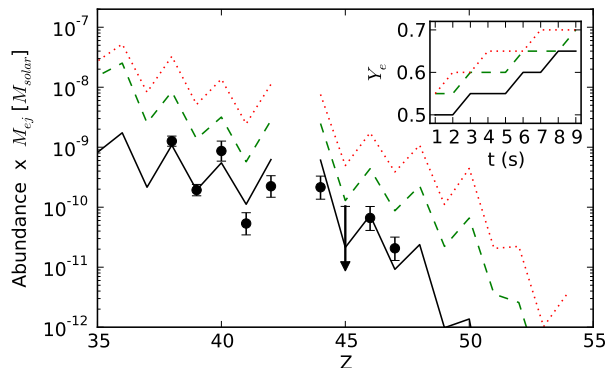


Fig. 7.— Integrated abundances in model 15M using the three different  $Y_e$  evolutions shown in the inset. Same colors and line styles are used for the abundances and  $Y_e$  evolutions. The LEPP pattern has been rescaled to fit the solid line abundances.

The main contribution to the integrated abundances come from mass elements ejected during the first seconds after bounce due to their large mass outflow. Late mass elements eject less mass but produce heavier elements because of the higher  $Y_e$ . These trends are shown in Fig. 8 by the mass-weighted abundances at 1 s and 9 s after bounce for two different initial  $Y_e$ . For  $Y_e = 0.5$  mainly iron-group nuclei are produced. LEPP elements can be synthesized for  $Y_e = 0.65$  as antineutrino absorption on free protons make possible  $(n, p)$  reactions. As high  $Y_e$  values are reached only by mass elements emitted at late times (small inset in Fig. 7), LEPP abundances are weighted by a lower mass ejection of the shell. Depending on the  $Y_e$  of the early mass elements, the amount of iron-group elements can change by orders of magnitude leading to large variations of the ratio between iron-group and LEPP elements.

While the LEPP elements are most probably produced during the neutrino-driven wind, the synthesis of iron-group nuclei occurs mainly in explosive nucleosynthesis when the supernova shock disrupts the stellar envelope (Woosley & Heger 2007). Therefore, the production of the iron-group elements in the neutrino-driven wind should be negligible. Although in our simulations iron-group elements are produced mostly when  $Y_e \approx 0.5$ , a higher  $Y_e$  combined



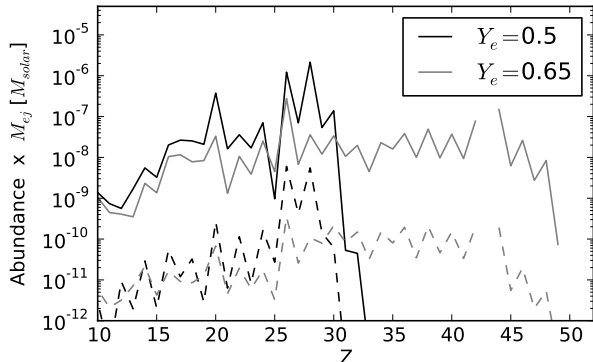


Fig. 8.— Abundances for the 15M trajectories ejected at 1 s (solid lines) and 9 s (dashed lines) after bounce assuming that the initial electron fraction is  $Y_e = 0.5$  (black lines) and  $Y_e = 0.65$  (grey lines).

with a lower neutrino luminosity may also produce them. In our model 15M, the abundances of iron-group elements (in particular,  $Z=29$ ) compared to observed abundances of HD 122563 (Westin et al. 2000) can constrain the  $Y_e$  of the early trajectories. We find that the  $Y_e$  evolution has to follow either a rapid increase so the amount of iron-group elements ejected stays low, or it has to start already at  $Y_e \gtrsim 0.55$  so there is only a minor production of these elements. The evolution represented by the solid line in Fig. 7 produces too much iron-group nuclei relative to LEPP elements as the  $Y_e$  stays close to 0.5 for several seconds. The evolutions represented by dotted and dashed lines are consistent with observations as the abundances of the iron-group elements are less than 10% of the observed abundances when normalizing to  $Z=39$ .

Production factors corresponding to different proton-rich evolutions are shown in Fig. 9. To gain some insight into the absolute abundances of LEPP elements, one may compare their abundances with the measured values of  $\alpha$ -elements that are the dominant products of core-collapse supernovae. For instance, Mg should take the value given by Eq. (10) since it is a typical supernova product. Assuming HD 122563 is representative for all supernovae and  $[\text{Mg}/\text{Y}]=0.9$  (Honda et al. 2004, 2006), one would expect the production factor of Y (single isotope) to be around 3. Figure 9 shows that  $P(\text{Y})$  has roughly the right value. Nevertheless, that some isotopes are over the production limit given by Eq. (10) means that either not all supernovae in the range  $8M_\odot < M < 25M_\odot$  reach the same proton-rich conditions or that the ejecta from our spherically symmetric, parametric model cannot be extrapolated to every supernova ejecta. If the abundances observed in HD 122563 are not representative of a typical supernovae ejecta then Y (or other LEPP elements) could be produced in different amounts. We find that abundances from models 10M and 25M behave very similar to 15M.

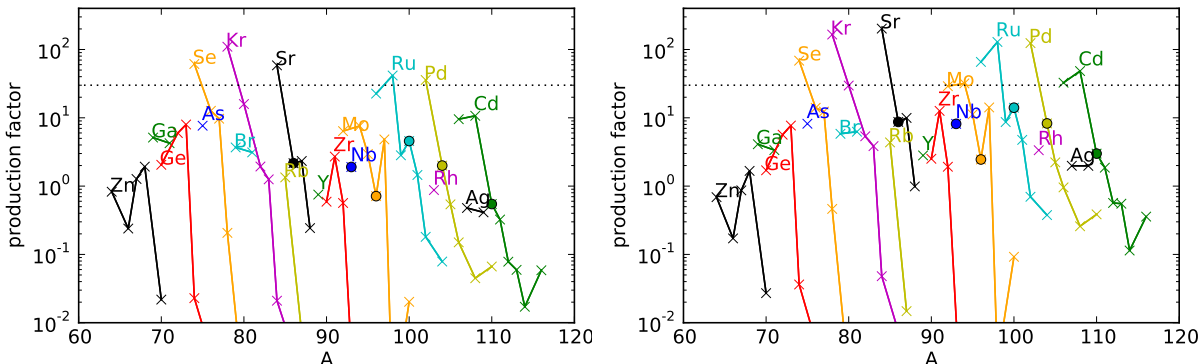


Fig. 9.— Production factors corresponding to the elemental abundances presented in Fig. 7 by the dashed and dotted lines are shown in the left and right panels, respectively. Almost only neutron-deficient isotopes (p-nuclei) are synthesized. The isotopes marked with circles are not produced in enough quantities in Travaglio et al. (2004).

For model 15M(s) is not possible to produce LEPP elements even when  $Y_e \sim 0.65$  due to the low entropy (Pruet et al. 2006). In addition, most of the abundances are on the proton-rich side of the valley of beta-stability (neutron-deficient isotopes). If the LEPP were responsible for the isotopic underabundances reported by Travaglio et al. (2004), proton-rich winds would not be enough to account for this contribution.

The nucleosynthesis dependance on neutrino luminosity is shown in Fig. 10 for a trajectory ejected 1 s after bounce with  $Y_e = 0.65$ . The neutrino luminosity obtained in Arcones et al. (2007) has been reduced by different factors. When the neutrino luminosity decreases the wind entropy has to increase (Eq. 1). For our test, we do not consider this dependence and keep the entropy (and other wind parameters) unchanged. Although, this is not fully consistent, it allows us to investigate the influence of the neutrino luminosity on the abundances separately from the effect of other wind parameters. We find that a reduction of the luminosity by a factor 2 (dashed line, “L/2”) leads to the production of only  $Z < 44$  elements. A factor of 5 reduction is enough to inhibit the production of any LEPP elements, as the flow can barely pass through the bottleneck at  $^{64}\text{Ge}$ . We note that previous nucleosynthesis studies based on the explosion model of Kitaura et al. (2006) do not produce LEPP elements (Hoffman et al. 2008; Wanajo et al. 2009) because the (anti)neutrino luminosity of this low mass progenitor ( $M = 8.8M_\odot$ ) is rather small and the expansion is very fast. Therefore, there are not enough neutrinos during sufficient time to get a successful  $\nu p$ -process. The neutrino luminosities obtained for heavier mass progenitors, as in our case and in Pruet et al. (2006) for a  $15 M_\odot$  progenitor, show that with higher luminosities the  $\nu p$ -process can occur in the supernova outflows. Although we have shown that with the

calculated (anti)neutrino luminosities it is possible to obtain the LEPP pattern, the neutrino luminosities from hydrodynamical simulations have large uncertainty and prevents us to draw definite conclusions.

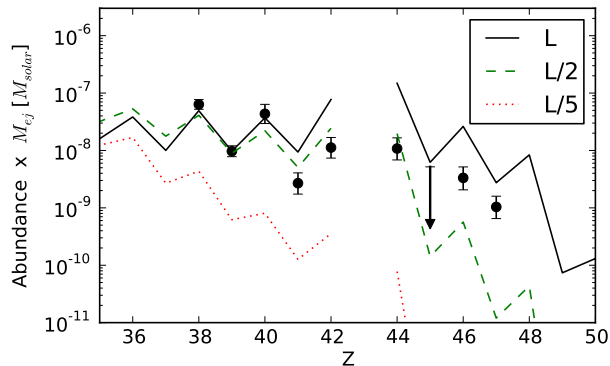


Fig. 10.— Abundance patterns obtained for the mass element ejected 1 s after bounce with  $Y_e = 0.65$  and different neutrino luminosity. Solid line shows the abundances using the luminosity from Arcones et al. (2007). For the other cases the luminosity has been reduced by different factors as indicated in the label.

### 3.2.2. Neutron-rich winds

Figure 11 shows integrated abundances for three possible neutron-rich  $Y_e$  evolutions (inset of the same Figure). When the  $Y_e$  decreases from 0.5 to 0.486, only  $Z \leq 40$  are produced (similar to Fig. 3). If  $Y_e$  decreases to 0.45, elements up to  $Z = 47$  can be produced. Contrary to proton-rich conditions, different  $Y_e$  evolutions lead to significant changes in the pattern. This sensitivity in the final abundances is due to the abrupt drop of the neutron abundance near  $Y_e = 0.5$  (shown in Fig. 5). This rapid change in neutron abundance is accompanied by a non-linear change in LEPP abundances when  $0.4 < Y_e < 0.5$  (shown in Fig. 6). Moreover, mass elements ejected at slightly different times (and therefore with small variations of the entropy and the expansion timescales) show a substantial difference on the neutron-to-seed ratio and subsequently on the abundances, making again difficult to get a robust pattern. Such strong dependence of the final abundances on the wind parameters is also found for the other models introduced in Sect. 3. In model 15M(s) the electron fraction has to be reduced down to  $Y_e \approx 0.4$  to produce elements up to  $Z = 47$ .

Production factors of the abundances shown by dashed and dotted lines in Fig. 11 are presented in the left and right panels of Fig. 12, respectively. Since in neutron-rich winds

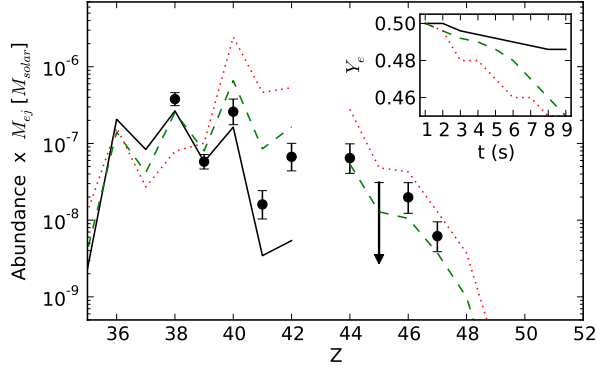


Fig. 11.— Same as Fig. 7 but for neutron-rich  $Y_e$  evolutions.

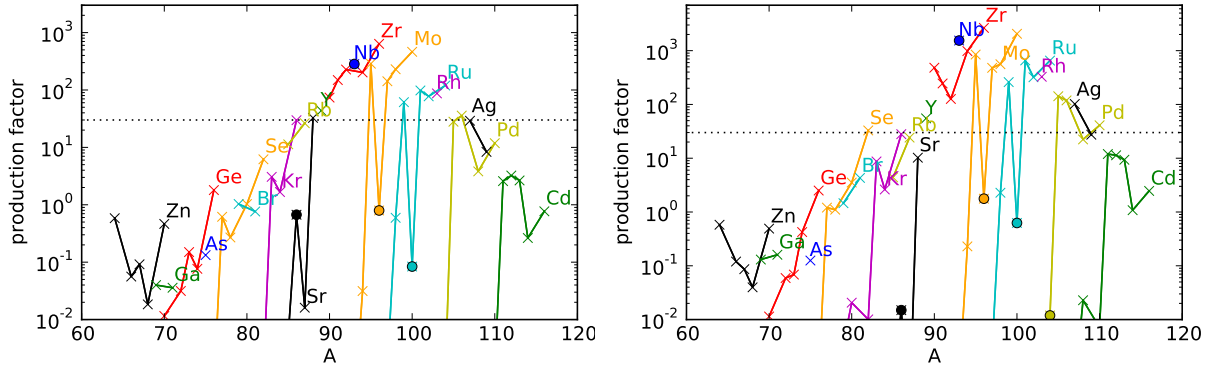


Fig. 12.— Production factors for two evolutions of the electron fraction: left panel correspond to green dashed line and right panel to the red dotted line in Fig. 11. The dotted horizontal line represents the upper limit above which isotopes are overproduced (see Sect. 3.1).

( $0.45 \lesssim Y_e < 0.5$ ) the amount of heavy nuclei produced is higher than in the proton-rich winds (Fig. 6), the overproduction around  $A = 90$  (related to the neutron magic number  $N = 50$ , Hoffman et al. (1996)) becomes a constraint. Similar to the conclusion reached for the proton-rich conditions, this suggests that not all mass ejected in neutrino-driven winds in core-collapse supernovae experience neutron-rich conditions. Previous results (see e.g., Woosley & Hoffman 1992; Woosley et al. 1994; Wittl et al. 1994; Hoffman et al. 1996; Freiburghaus et al. 1999; Hoffman et al. 2008) suggest that only a small amount of the mass ejected by core-collapse supernovae can be neutron-rich. It is possible that the neutron richness of the ejecta depends on progenitor mass because more massive stars lead to more compact neutron stars and thus higher neutrino energies, which may favour neutron-rich conditions. A different alternative to avoid the overproduction is to have anisotropic explosions

with an electron fraction distribution in the ejecta that achieves neutron-rich conditions only in some regions. Recent two-dimensional supernova simulations present proton-rich ejecta with neutron-rich blobs or pockets that contain only a small mass (Wanajo et al. 2010b).

Further investigations are necessary to conclude which of the possibilities addressed here can explain the observations of LEPP elements in UMP stars. Based on spherical symmetric simulations we have showed that it is possible to reproduce the LEPP elemental pattern under different wind conditions. Multidimensional simulations will determine the effect of anisotropic  $Y_e$  distribution on the wind nucleosynthesis. Such multidimensional simulations combined with exploratory studies like ours will provide constraints for the specific conditions (e.g.,  $Y_e$  evolution) and for the overall contribution of neutron- and proton-rich winds to the solar system inventory. Using our results, it is hard to obtain the solar LEPP pattern (Travaglio et al. 2004; Montes et al. 2007) by combining neutron- and proton-rich conditions. Moreover, Galactic chemical evolution models are necessary before a definite conclusion can be drawn to the exact contribution of core-collapse supernovae to the solar systems abundances.

#### 4. Conclusions and summary

We have performed nucleosynthesis calculations based on spherically symmetric supernova simulations (Arcones et al. 2007) which include efficient neutrino transport and follow the evolution of the ejecta from a few milliseconds to several seconds after bounce during the neutrino-driven wind phase. The integrated nucleosynthesis was analyzed for different stellar progenitors with masses of 10, 15, and 25  $M_\odot$ . We have found that light element primary process abundances can be produced under realistic conditions in the neutrino-wind phase. No heavy r-process elements can be synthesized under those conditions (see also Roberts et al. 2010; Wanajo et al. 2010b).

Our results indicate that the nucleosynthesis occurring in neutrino-driven winds does not depend significantly on the progenitor, but rather on the proto-neutron star evolution which in turn directly affects nucleosynthesis-relevant wind parameters (Qian & Woosley 1996) such as entropy, expansion timescale, and electron fraction. The electron fraction depends on neutrino properties which are determined by the still uncertain neutrino interactions and transport. Since the calculation of the electron fraction remains challenging (Hüdepohl et al. 2010) the impact of the electron fraction on the production of LEPP elements was studied. The LEPP pattern obtained by Qian & Wasserburg (2007); Montes et al. (2007) was reproduced for different evolutions of the electron fraction towards proton- and neutron-rich conditions.

The LEPP pattern reproduced in proton-rich winds was found to be robust under small variations in the evolution wind parameters. Nevertheless, elements heavier than iron-group nuclei can only be produced when the neutrino fluxes are high enough to allow for a successful  $\nu$ p-process. The amount of heavy elements ejected is rather low since most of the outflow matter consists of protons and  $\alpha$ -particles. Although the elemental abundances nicely reproduce the observed LEPP pattern, mainly neutron-deficient isotopes are produced (see also Fröhlich et al. 2006a,b; Wanajo et al. 2010a). Therefore, proton-rich conditions can explain the LEPP elements observed in UMP stars but not in the missing isotopic underabundances in the solar system (Travaglio et al. 2004).

When the electron fraction is assumed to evolve towards neutron-rich conditions, the LEPP pattern can be also reproduced but it is not robust under small variations of the wind parameters. We find an overproduction around  $A \sim 90$  that was already pointed out in previous nucleosynthesis studies (Woosley & Hoffman 1992; Woosley et al. 1994; Wittl et al. 1994; Freiburghaus et al. 1999; Hoffman et al. 2008). This overproduction and the fact that most recent supernova simulations (Fischer et al. 2010; Hüdepohl et al. 2010) favor proton-rich winds could suggest that neutron-rich winds are rare events. Scenarios that could explain the ejection of only a small amount of neutron-rich material include 1) very small pockets with neutron-rich material that may appear in multidimensional simulations (Wanajo et al. 2010b); 2) neutron-rich conditions that can only be obtained at very late times when the amount of ejected mass is very small; 3) there is only a small subset of all supernovae that can develop neutron-rich winds.

The isotopic underabundances reported by (Travaglio et al. 2004) cannot be reproduced based in our models without overproducing other isotopes. Evolving from proton to neutron conditions in the wind does not resolve the overproduction, which could be a hint of the limitation of our models. However, this can also suggest deficiencies in the s-process model used by (Travaglio et al. 2004). We cannot conclude whether the solar and the UMP stars LEPP abundances are produced by the same light element primary process.

Observation of isotopic abundances in UMP stars would constrain the evolution of the electron fraction and thus of the neutrino properties in supernovae. In addition more work is necessary in improving long-time supernova models (e.g., multidimensional simulations, more accurate treatment of neutrino reactions and transport) and also the experimental and theoretical nuclear reactions relevant in the wind nucleosynthesis before definite conclusions can be reached.

We thank H. Th. Janka, K. Langanke, G. Martínez-Pinedo, H. Schatz, and F. K. Thielemann for stimulating discussions. We are grateful to G. Martínez-Pinedo for providing us the

nucleosynthesis network. A. Arcones acknowledges support of the Deutsche Forschungsgemeinschaft through contract SFB 634, ExtreMe Matter Institute EMMI, and Swiss National Science Foundation. F. Montes is supported by NSF grants PHY 08-22648 (Joint Institute for Nuclear Astrophysics) and PHY 01-10253.

## REFERENCES

- Angulo, C., Arnould, M., Rayet, M., Descouvemont, P., Baye, D., Leclercq-Willain, C., Coc, A., Barhoumi, S., Aguer, P., Rolfs, C., et al., 1999, *Nucl. Phys. A*, 656, 3
- Aoki, W., Honda, S., Beers, T. C., Kajino, T., Ando, H., Norris, J. E., Ryan, S. G., Izumiura, H., Sadakane, K., & Takada-Hidai, M., 2005, *ApJ*, 632, 611
- Arcones, A., Janka, H.-T., & Scheck, L., 2007, *A&A*, 467, 1227
- Arcones, A., & Janka, H.-T., 2011, *A&A*, 526, A160
- Arcones, A., Martínez-Pinedo, G., O’Connor, E., Schwenk, A., Janka, H.-T., Horowitz, C. J., & Langanke, K., 2008, *Phys. Rev. C*, 78, 015806
- Arcones, A., Martínez-Pinedo, G., Roberts, L. F., & Woosley, S. E., 2010, *A&A*, 522, A25
- Arnould, M., Goriely, S., & Takahashi, K., 2007, *Phys. Repts.*, 450, 97
- Busso, M., Gallino, R., & Wasserburg, G. J., 1999, *ARA&A*, 37, 239
- Cameron, A. G. W., 2001, *ApJ*, 562, 456
- , 2003, *ApJ*, 587, 327
- Cappellaro, E., Evans, R., & Turatto, M., 1999, *A&A*, 351, 459
- Duncan, R. C., Shapiro, S. L., & Wasserman, I., 1986, *ApJ*, 309, 141
- Fischer, T., Whitehouse, S. C., Mezzacappa, A., Thielemann, F., & Liebendörfer, M., 2010, *A&A*, 517, A80
- Freiburghaus, C., Rembges, J.-F., Rauscher, T., Kolbe, E., Thielemann, F.-K., Kratz, K.-L., Pfeiffer, B., & Cowan, J. J., 1999, *ApJ*, 516, 381
- Fröhlich, C., Hauser, P., Liebendörfer, M., Martínez-Pinedo, G., Thielemann, F.-K., Bravo, E., Zinner, N. T., Hix, W. R., Langanke, K., Mezzacappa, A., et al., 2006a, *ApJ*, 637, 415

- Fröhlich, C., Martínez-Pinedo, G., Liebendörfer, M., Thielemann, F.-K., Bravo, E., Hix, W. R., Langanke, K., & Zinner, N. T., 2006b, *Phys. Rev. Lett.*, 96, 142502
- Hoffman, R. D., Müller, B., & Janka, H.-T., 2008, *ApJ*, 676, L127
- Hoffman, R. D., Woosley, S. E., Fuller, G. M., & Meyer, B. S., 1996, *ApJ*, 460, 478
- Hoffman, R. D., Woosley, S. E., & Qian, Y.-Z., 1997, *ApJ*, 482, 951
- Honda, S., Aoki, W., Kajino, T., Ando, H., Beers, T. C., Izumiura, H., Sadakane, K., & Takada-Hidai, M., 2004, *ApJ*, 607, 474
- Honda, S., Aoki, W., Ishimaru, Y., Wanajo, S., & Ryan, S. G., 2006, *ApJ*, 643, 1180
- Horowitz, C. J., & Li, G., 1999, *Phys. Rev. Lett.*, 82, 5198
- Hüdepohl, L., Müller, B., Janka, H., Marek, A., & Raffelt, G. G., 2010, *Phys. Rev. Lett.*, 104, 251101
- Ishimaru, Y., & Wanajo, S., 1999, *ApJ*, 511, L33
- Ishimaru, Y., Wanajo, S., Aoki, W., & Ryan, S. G., 2004, *ApJ*, 600, L47
- Jaikumar, P., Meyer, B. S., Otsuki, K., & Ouyed, R., 2007, *A&A*, 471, 227
- Janka, H.-T., Langanke, K., Marek, A., Martínez-Pinedo, G., & Müller, B., 2007, *Phys. Repts.*, 442, 38
- Johnson, J. A., & Bolte, M., 2002, *ApJ*, 579, 616
- Kifonidis, K., Plewa, T., Scheck, L., Janka, H.-T., & Müller, E., 2006, *A&A*, 453, 661
- Kitaura, F. S., Janka, H.-T., & Hillebrandt, W., 2006, *A&A*, 450, 345
- Lattimer, J. M., & Swesty, F. D., 1991, *Nucl. Phys. A*, 535, 331
- Lodders, K., 2003, *ApJ*, 591, 1220
- Marek, A., Dimmelmeier, H., Janka, H.-T., Müller, E., & Buras, R., 2006, *A&A*, 445, 273
- Martinez-Pinedo, G., Kelic, A., Langanke, K., Schmidt, K., Mocerlj, D., Fröhlich, C., Thielemann, F., Panov, I., Rauscher, T., Liebendörfer, M., et al., 2006, in *International Symposium on Nuclear Astrophysics - Nuclei in the Cosmos*
- Mathews, G. J., Bazan, G., & Cowan, J. J., 1992, *ApJ*, 391, 719



- Messer, O. E. B., Liebendörfer, M., Hix, W. R., Mezzacappa, A., & Bruenn, S. W., 2003, in *From Twilight to Highlight: The Physics of Supernovae*, p. 70
- Meyer, B. S., Mathews, G. J., Howard, W. M., Woosley, S. E., & Hoffman, R. D., 1992, *ApJ*, 399, 656
- Mezzacappa, A., Liebendörfer, M., Bronson Messer, O. E., Raphael Hix, W., Thielemann, F.-K., & Bruenn, S. W., 2001, *Phys. Rev. Lett.*, 86, 1935
- Möller, P., Nix, J. R., & Kratz, K.-L., 1997, *At. Data Nucl. Data Tables*, 66, 131
- Montes, F., Beers, T. C., Cowan, J., Elliot, T., Farouqi, K., Gallino, R., Heil, M., Kratz, K., Pfeiffer, B., Pignatari, M., et al., 2007, *ApJ*, 671, 1685
- Nordhaus, J., Burrows, A., Almgren, A., & Bell, J., 2010, *ApJ*, 720, 694
- NuDat2, 2009, "National Nuclear Data Center, information extracted from the NuDat 2 database", <http://www.nndc.bnl.gov/nudat2/>
- Otsuki, K., Honda, S., Aoki, W., Kajino, T., & Mathews, G. J., 2006, *ApJ*, 641, L117
- Otsuki, K., Tagoshi, H., Kajino, T., & Wanajo, S., 2000, *ApJ*, 533, 424
- Ouyed, R., Dey, J., & Dey, M., 2002, *A&A*, 390, L39
- Pruet, J., Hoffman, R. D., Woosley, S. E., Janka, H.-T., & Buras, R., 2006, *ApJ*, 644, 1028
- Qian, Y.-Z., & Wasserburg, G. J., 2001, *ApJ*, 559, 925
- Qian, Y.-Z., & Wasserburg, G. J., 2007, *Phys. Rep.*, 442, 237
- , 2008, *ApJ*, 687, 272
- Qian, Y.-Z., & Woosley, S. E., 1996, *ApJ*, 471, 331
- Rampp, M., & Janka, H.-T., 2000, *ApJ*, 539, L33
- Rauscher, T., & Thielemann, F.-K., 2000, *At. Data Nucl. Data Tables*, 75, 1
- Roberts, L. F., Woosley, S. E., & Hoffman, R. D., 2010, *ApJ*, 722, 954
- Scheck, L., Kifonidis, K., Janka, H.-T., & Müller, E., 2006, *A&A*, 457, 963
- Shen, H., Toki, H., Oyamatsu, K., & Sumiyoshi, K., 1998, *Nucl. Phys. A*, 637, 435
- Snedden, C., Cowan, J. J., & Gallino, R., 2008, *ARA&A*, 46, 241

- Sneden, C., Cowan, J. J., Lawler, J. E., Ivans, I. I., Burles, S., Beers, T. C., Primas, F., Hill, V., Truran, J. W., Fuller, G. M., et al., 2003, *ApJ*, 591, 936
- Straniero, O., Gallino, R., & Cristallo, S., 2006, *Nuclear Physics A*, 777, 311
- Thompson, T. A., Burrows, A., & Meyer, B. S., 2001, *ApJ*, 562, 887
- Travaglio, C., Gallino, R., Arnone, E., Cowan, J., Jordan, F., & Sneden, C., 2004, *ApJ*, 601, 864
- Truran, J. W., & Cowan, J. J., 2000, Proceedings of the 10th workshop on "Nuclear Astrophysics", 64
- Truran, J. W., Cowan, J. J., Pilachowski, C. A., & Sneden, C., 2002, *PASP*, 114, 1293
- Wanajo, S., 2006, *ApJ*, 647, 1323
- Wanajo, S., 2007, *ApJ*, 666, L77
- Wanajo, S., Janka, H., & Kubono, S., 2010a, arXiv:, 1004.4487
- Wanajo, S., Janka, H., & Müller, B., 2010b, *ApJ*, 726, L15
- Wanajo, S., Nomoto, K., Janka, H., Kitaura, F. S., & Müller, B., 2009, *ApJ*, 695, 208
- Wasserburg, G. J., Busso, M., & Gallino, R., 1996, *ApJ*, 466, L109
- Westin, J., Sneden, C., Gustafsson, B., & Cowan, J. J., 2000, *ApJ*, 530, 783
- Witti, J., Janka, H.-T., & Takahashi, K., 1994, *A&A*, 286, 841
- Woosley, S. E., & Heger, A., 2007, *Phys. Rep.*, 442, 269
- Woosley, S. E., & Hoffman, R. D., 1992, *ApJ*, 395, 202
- Woosley, S. E., Wilson, J. R., Mathews, G. J., Hoffman, R. D., & Meyer, B. S., 1994, *ApJ*, 433, 229